Science of the Total Environment 719 (2020) 137493

Contents lists available at ScienceDirect

Science of the Total Environment

journal homepage: www.elsevier.com/locate/scitotenv

Characteristics of peroxyacetyl nitrate (PAN) in a coastal city of southeastern China: Photochemical mechanism and pollution process

Baoye Hu [a,b,c], Taotao Liu [a,b,c], Youwei Hong [a,b,*], Lingling Xu [a,b], Mengren Li [a,b], Xin Wu [a,b,c], Hong Wang [d], Junhuai Chen [a,b], Jinsheng Chen [a,b,*]

[a] Center for Excellence in Regional Atmospheric Environment, Institute of Urban Environment, Chinese Academy of Sciences, Xiamen 361021, China
[b] Key Lab of Urban Environment and Health, Institute of Urban Environment, Chinese Academy of Sciences, Xiamen 361021, China
[c] University of Chinese Academy of Sciences, Beijing 100086, China
[d] Fujian Meteorological Science Institute, Fuzhou 350001, China

HIGHLIGHTS

- Continuous field observation on peroxyacetyl nitrate (PAN) was conducted.
- It was proved that OH radicals can replace the role of UV in PAN formation.
- PAN was easy to accumulate in winter in $PM_{2.5}$ with concentration ≥ 35 μg·m^{-3}.

GRAPHICAL ABSTRACT

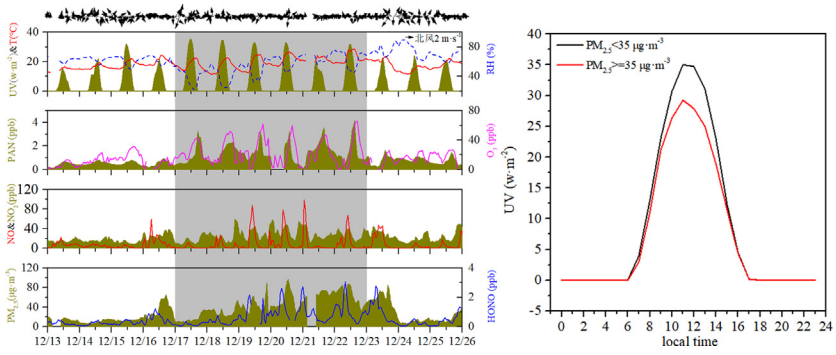

ARTICLE INFO

Article history:
Received 30 October 2019
Received in revised form 20 February 2020
Accepted 20 February 2020
Available online 21 February 2020

Editor: Pingqing Fu

Keywords:
Peroxyacetyl nitrate (PAN)
Coastal city
Southeastern China
Photochemical mechanism
Pollution process

ABSTRACT

Peroxyacetyl nitrate (PAN) can effectively indicate photochemical pollution, and also plays a vital role in regional oxidant balance. One-year continuous monitoring of PAN in a coastal city of southeastern China was investigated. The mean concentration of PAN in winter (0.64 ppb) was close to that in autumn (0.73 ppb), indicating that photochemical pollution was still non-negligible in the cold season. The peak occurrence time between O_3 and PAN had a delay of 1–2 h in four seasons, due to the rapid decomposition rate of PAN in midday. Emission sources of the precursors are located to the south of the monitoring site, so high concentrations of PAN and O_3 are frequently observed under southerly wind conditions. The air mass with low concentration of PAN (0.22–0.34 ppb) and O_3 (18.17–23.67 ppb) originated from the ocean with less anthropogenic air pollutants. Continental air mass with high PAN concentration might be related to the contribution of heterogeneous reactions of $PM_{2.5}$ to the promotion of PAN formation. In the polluted case, PAN concentration was often higher than 1.0 ppb and reached the peak of 4.2 ppb, suggesting the influence of photochemical reactions and local accumulation. High concentrations of HONO and sufficient ultraviolet radiation might be the main factors for rapid photochemical production of PAN. Besides, the lifetime of PAN in winter under the condition of high $PM_{2.5}$ concentration (≥35 μg·m^{-3}) was up to 3.246 days. This study provided insights into photochemical mechanism and pollution process in a coastal city of southeastern China.

* Corresponding authors at: Center for Excellence in Regional Atmospheric Environment, Institute of Urban Environment, Chinese Academy of Sciences, Xiamen 361021, China.
E-mail addresses: ywhong@iue.ac.cn (Y. Hong), jschen@iue.ac.cn (J. Chen).

https://doi.org/10.1016/j.scitotenv.2020.137493
0048-9697/

1. Introduction

Peroxyacyl nitrate (PAN), the product of the combination of peroxyacetyl radical (PA) and nitrogen dioxide (NO_2), can effectively indicate photochemical pollution (Xue et al., 2014; Han et al., 2017; Qiu et al., 2019). And OH radical oxidation or photolysis of acetaldehyde, methylglyoxal, and acetone is the dominant sources of PA (Han et al., 2017). PAN decomposes and generates NO_2 in a warm environment, which is the important source of nitrogen oxides (NOx) in areas with few anthropogenic sources. Although the concentration of PAN in the surface atmosphere is much lower than that of ozone (O_3), the phytotoxicity of PAN is much greater than that of O_3 (Temple and Taylor, 1983). Besides, PAN does harm to humans and animals.

In recent years, a number of studies of PAN have conducted in China. However, most of them focused on the severe photochemical smog episodes. For example, Zhang et al. (2019) conducted a discontinuous observation on PAN pollution characteristics in Beijing with severe haze events. Zeng et al. (2019) carried out a short-term field measurement in suburban of Hong Kong from October to November 2016 on atmospheric lifetime of PAN and its effect on local O_3 pollution. Xu et al. (2018) investigated the impacts of planetary boundary layer (PBL) evolution and transport processes on PAN characteristics in remote area based on field observation 17–24 August 2011 and 15 May to 13 July 2012. These studies were only a few months or even weeks, which were not enough to draw a full picture and fate of PAN. In addition, few researchers reported continuous observation PAN on remote area (Wang et al., 2015). And photochemical parameters should be simultaneously measured to determine their effects on the formation of PAN, especially in urban areas (Zhang et al., 2014).

Xiamen is located in the southeastern coast of China, where severe photochemical pollution episodes occur frequently. It belongs to the subtropical monsoon climate, and has a warm and wet climate with 23.32 °C mean of temperature and 77.66% mean of relative humidity. The maximum wind speed can reach 10.3 $m \cdot s^{-1}$. The cold and dry air masses carried by northerly from inland dominate in autumn and winter, while the prevailing air masses in the late of spring and summer are southerly characterized by warm and wet. According to the Municipal Bureau of Statistics (http://tjj.xm.gov.cn/tjzl/), Xiamen covered an area of 1700.61 km^2 and had a population of 4.11 million. Number of motor vehicles reached to 1,572,088 in 2018, which is 2.73 times that in 2008. The emissions of NOx and volatile organic compounds (VOCs) in 2009 were estimated to be 5.28×10^4 and 6.06×10^4 t, respectively (Lu et al., 2014). The annual sunshine time reached 2233.50 h. High concentration of precursors and long sunshine time are in favor of serious photochemical pollution in this region. Therefore, Xiamen is an ideal place for studying the effects of transport and local production on photochemical pollution. In this study, continuous measurement of PAN was conducted at Institute of Urban Environment, Chinese Academy of Sciences (IUE, CAS) to understand its seasonal variation and sources, then to characterize the effect of PM2.5 on PAN local generation.

In this study, we presented a comprehensive set of measurements, including PAN, O_3, and some related species from Jan. to Dec. 2018, which constructed a specific campaign to study the characteristic and fate of PAN. The purpose of this study was to (1) evaluate the temporal variation of PAN, and its correlation with precursors and meteorological parameters, (2) identify the transport pathways and corresponding pollutants concentration by cluster analysis of backward trajectories, (3) analyze a severe photochemical episode occurred during 17–22 December 2018 for better understanding the local formation mechanism of PAN.

2. Methods

2.1. Site

The monitoring site is located on the rooftop of a 20-floor building of IUE (118.06°E, 24.61°N) in Xiamen, China, which is 80 m above the ground. The site is not susceptible to the underlying surface at a height of 80 m, which is conducive to the study of region transport. IUE is almost located on the middle of Xiamen (Fig. 1). This site was characterized by a rapidly urbanizing development area surrounded by highways, educational institutions, and residential buildings. As shown in Fig. 1, Xiamen island with densely populated and traffic jams was located at the upwind of IUE when the wind direction was dominated by southerly winds.

2.2. Instruments and data collection

PAN concentration was determined through a PAN analyzer (PANs-1000, Focused Photonics Inc., Hangzhou, China) consisted by gas chromatography (GC) with electron capture detector (ECD). The specific workflow is as follows: air sample or calibrate sample is controlled by the three-way solenoid value powered by a sampling pump. In the sampling mode, the sample is filtered by PTFE microporous membrane, and then enters the loop through the six-way valve. After the sampling is done, switch through the six-way valve to start the sample injection. In the injection mode, the loop is connected to the carrier gas path, and the sample is separated after the carrier gas enters the column. The separated components are sent to the detector, and the electrical signals are recorded and transferred to the concentration of PAN. In the calibration mode, the flow rate of acetone and NO is separately controlled by Mass Flow Controller (MFC), and the PAN standard gas is generated by ultraviolet light irradiation. The zero gas flow is controlled by MFC, and the sample is diluted to the required calibration concentration for injection analysis. Multi-point calibration was conducted once a month, and single-point calibration was conducted every week. PAN was detected every 5 min and the detection limit was 50 ppt. The uncertainty and precision of PAN measurement were $\pm$ 10% and 3%, respectively.

HONO concentrations were measured by the Incoherent Broadband Cavity Enhanced Absorption Spectroscopy (IBBCEAS). This technique is based on the Lambert Beer absorption law, and the principle for HONO measurement has been reported (Duan et al., 2018). The detection limit of HONO was 100 ppt at a time resolution of 1 min. The system was calibrated using high purity nitrogen (99.999%) gas to replace the light spectrum twice a day. Criteria air pollutants including O_3, NOx, and CO were determined by ultraviolet radiation (UV) absorption (TEI model 49i), chemiluminescence with a molybdenum converter (TEI model 42i) and non-dispersive infrared (TEI model 48i), respectively. The measurements and calibrations were made according to the guidelines of instruments procedure. The detection limits of O_3, NOx, and CO were 1, 0.5, 40 ppb, respectively. An oscillating microbalance with tapered element (TEOM1405, Thermo Scientific Corp., MA, US) was used to monitor particulate matters (PM_{10} and $PM_{2.5}$). When the loading of filters was above 90%, the tape was replaced to guarantee accuracy of measurement. Meteorological parameters such as wind direction (WD), wind speed (WS), relative humidity (RH) and temperature (T), were measured by an ultrasonic atmospherium (150WX, Airmar, the USA). Photolysis frequencies of HONO and NO_2 were derived from actinic flux measurements from a photolysis spectrometer developed by China's Focused Photonics Inc. cooperating with Peking University.

2.3. Air trajectories analysis

The Global Data Assimilation System (GDAS) data were applied to calculate 72 h backward air trajectories with every hour ending at 500 m a.s.l. GDSA data were collected from National Oceanic and Atmospheric Administration (NOAA) Air Resources Laboratory (ARL) (ftp://arlftp.arlhq.noaa.gov./pub/archives/gdas1).

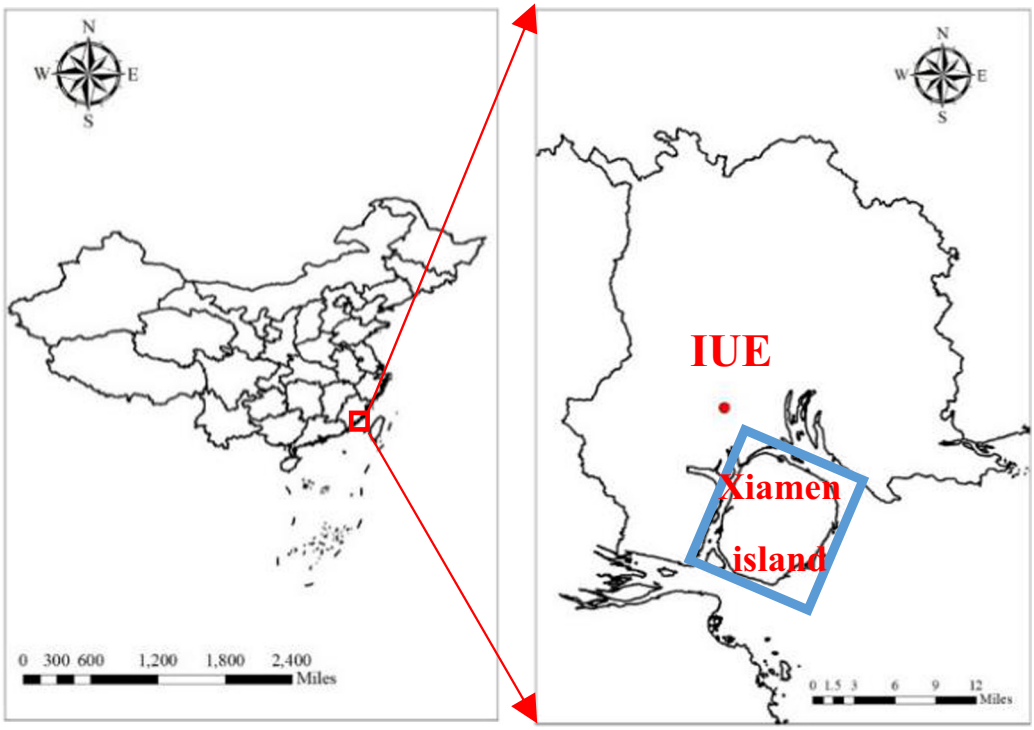

Fig. 1. Location of Xiamen in China (left) and location of monitoring site in Xiamen (right).

3. Results and discussion

3.1. Overviews of PAN

The mean concentration of PAN measured at the monitoring site was 0.55 ppb (Table 1). Compared with the guideline from World Health Organization (WHO, 1987), the concentration of PAN in this study was relatively low, except for one single hourly data monitored at IUE (4.19 ppb (22 Dec., 15:00)). WHO (1987) recommends PAN's air quality guidelines to be 5 ppb to avoid vegetation damage. However, it was reported by WHO (1996) that even several ppb PAN is very poisonous to human. Moreover, quantifying the regional PAN concentration is still important because it acts in long-range transport of atmospheric reactive nitrogen (Singh et al., 1986). Table 1 summarized the concentration of PAN previously measured at different kinds of sites. In this study, PAN concentration was higher than those in remote sites and regional background, but similar to those in Jeju Island, Korea. However, PAN concentration in Xiamen was lower than those measured in Seoul, Korea and inland cities in China, such as Lanzhou, Tianjin, and Beijing. Similar PAN concentrations (0.36–0.44 ppb) at remote/background sites in different cities indicated its non-negligible background value (Xu et al., 2018).

3.2. Temporal pattern of PAN and O_3

3.2.1. Seasonal distribution

PAN concentration and relevant parameters (including O_3, PAN/O_3, NO, NO_2, UV, T and rainfall) were summarized in Table 2. One-way analysis of variance (ANOVA) was preferentially conducted to distinguish seasonal variations of various parameters. Spring included March, April and May; summer included June, July and August; autumn included September, October and November; winter included December, January and February. The mean concentration of PAN in autumn was significantly higher than all other seasons. However, the relatively higher PAN concentration (0.64 ppb) in winter indicated that photochemical pollution was still non-negligible in coastal area of southeast China. The main sink of PAN is thermal degradation (Mellouki et al., 2015; Sillman, 1995). The thermal decomposition rate of PAN not only depends on temperature but also on the ratio of NO to NO_2. There was no significant difference

Table 1
Comparison of PAN concentrations with other studies.

City	Site description	Period	Mean (ppb)	Ref.
Xiamen, China	Suburban	Jan.–Dec. 2018	0.55	This study
Hongkong, China	Suburban	Oct.–Nov. 2016	0.63	(Zeng et al., 2019)
Lanzhou, China	Suburban	Jun.–Jul. 2006	0.76	(Zhang et al., 2009)
Mt. Waliguan, China	Remote	Jul.–Aug. 2006	0.44	
Tianjin, China	Urban	Jul.–Aug. 2017	0.73	(Yao et al., 2019)
Jinan, China	Urban	Nov. 2015–Jan. 2016	1.89	(Liu et al., 2018)
		Apr. 2016–Jul. 2016	2.54	
Beijing, China	Suburban	Jun.–Sep. 2010	2.61	(Zhang et al., 2015)
Beijing, China	Suburban	Dec. 2015–Mar. 2016	1.04	(Zhang et al., 2019)
Tibetan Plateau, China	Remote	Aug. 2011	0.36	(Xu et al., 2018)
		May–Jul. 2012	0.44	
Jeju Island, Korea	Suburban	Oct.–Nov. 2010	0.6	(Han et al., 2017)
Seoul, Korea	Urban	May–Jun. 2004, May–Jun. 2005	0.8	(Lee et al., 2008)
Baengyeong Island, South Korea	Regional background	Aug. 2010, Oct. 2010, Jan. 2011, Mar. 2011	0.38	(Lee et al., 2012)
Seoul, South Korea	Urban	Jan.–Dec. 2011	0.61	(Lee et al., 2013)

Table 2
Summary of mean PAN, related pollutants and meteorological parameters during a full year period in 2018.

	PAN (ppb)	O_3 (ppb)	PAN/O_3	NO (ppb)	NO_2(ppb)	UV ($W \cdot m^{-2}$)	T (°C)	Rainfall (mm)
Spring	0.50 b	31.24c	0.06a	5.87b	17.04c	10.65c	23.92b	176.80b
Summer	0.35a	26.66 b	0.04a	3.49 a	11.22a	11.70d	30.00d	495.60d
Autumn	0.73d	32.32c	0.04a	3.29a	16.44b	9.22b	25.33c	148.40a
Winter	0.64c	22.17a	0.14b	6.15b	17.64d	6.31a	15.81a	228.20c
Year	0.55	28.11	0.07	4.69	15.56	9.42	23.60	1049.00

Note: Different lowercase letters represented significant differences between seasons (0.05).

of the ratio of NO/NO_2 between summer (0.19) and winter (0.20). Therefore, the least amount of PAN (0.04 ppb) in winter was removed by thermal degradation, due to the lowest temperature (15.81 °C) in winter. However, mean concentration of O_3 in winter was significantly lower than all other seasons, indicating the impact of weak photochemical reaction under the minimum ultraviolet radiation (UV) conditions and the strong NO titration. Therefore, the ratio of PAN/O_3 in winter was significantly higher than all other seasons. Although UV was the strongest in summer, the rainfall was the largest (495.60 mm), accounting for 47.24% of the annual rainfall (1049.00 mm) (data from http://tjj.xm.gov.cn/tjzl/).In addition, affected by the East Asian monsoon, the air mass in summer was mainly from the ocean, and the concentration of PAN and O_3 at the monitoring site was diluted (Hu et al., 2019; Tanimoto, 2002; Xie et al., 2016).These results would be discussed in Section 3.5.

3.2.2. Diurnal variation

Mean diurnal concentrations of PAN, O_3 and related parameters in spring, summer, autumn and winter were shown in Fig. 2 a, b, c and d, respectively. The concentration of PAN and O_3 started to rise at 07:00 in spring (Fig. 2a). PAN peaked at 14:00 with 1.10 ppb and started to decrease in the afternoon. In contrast, the averaged concentration (59.08 ppb) of O_3 peaked at 15:00. As shown in Fig. 2b, PAN and O_3 in summer peaked at 12:00 and 14:00, respectively, both peaking earlier compared with spring. The mean mixing ratios of PAN and O_3 in summer had a maximum of 0.93 and 55.46 ppb, respectively, both being lower than those in spring. Fig. 2c showed that PAN peaked at 14:00 with 1.24 ppb, and O_3 peaked at 16:00 with 52.54 ppb in autumn. Fig. 2d showed that PAN peaked at 15:00 with 0.98 ppb, and O_3 peaked at 16:00 with 35.18 ppb in winter. There was 1–2 h time in advance the peak occurrence between PAN and O_3 in four seasons, probably due to the decomposition rate of PAN increased with the increase of temperature. Similar result was found in Lanzhou, China in summer (Zhang et al., 2009). However, the peak of PAN concentration in winter was late compared with the peak of O_3 concentration in Beijing (Zhang, 2013). The thermal degradation rate of PAN was low, due to the low temperature in winter. Moreover, rich VOCs had a certain effect on the accumulation of PA radicals, which could rapidly react with high concentration of NO_2. When the PAN generation rate was higher than its consumption rate, the PAN concentration continued to rise, so the peak appeared later. This was the reason why PAN peak appeared at the latest in winter and at the earliest in summer in this study. The variation between maximum and minimum values of PAN in summer was the highest (0.82 ppb) while is the smallest difference in winter (0.56 ppb). This variation reflected the net growth pattern of PAN. The net growth of PAN is relatively low in winter. The lifetime of PAN was extended when the temperature decreased. PAN was actively formed during the day under strong UV conditions, and rapidly decomposed at night with high temperature in summer.

3.3. Correlations between PAN and O_3 concentrations

As the products of photochemical source involving NOx and VOCs, PAN and O_3 generally have a relatively close relationship (Rubio et al.,

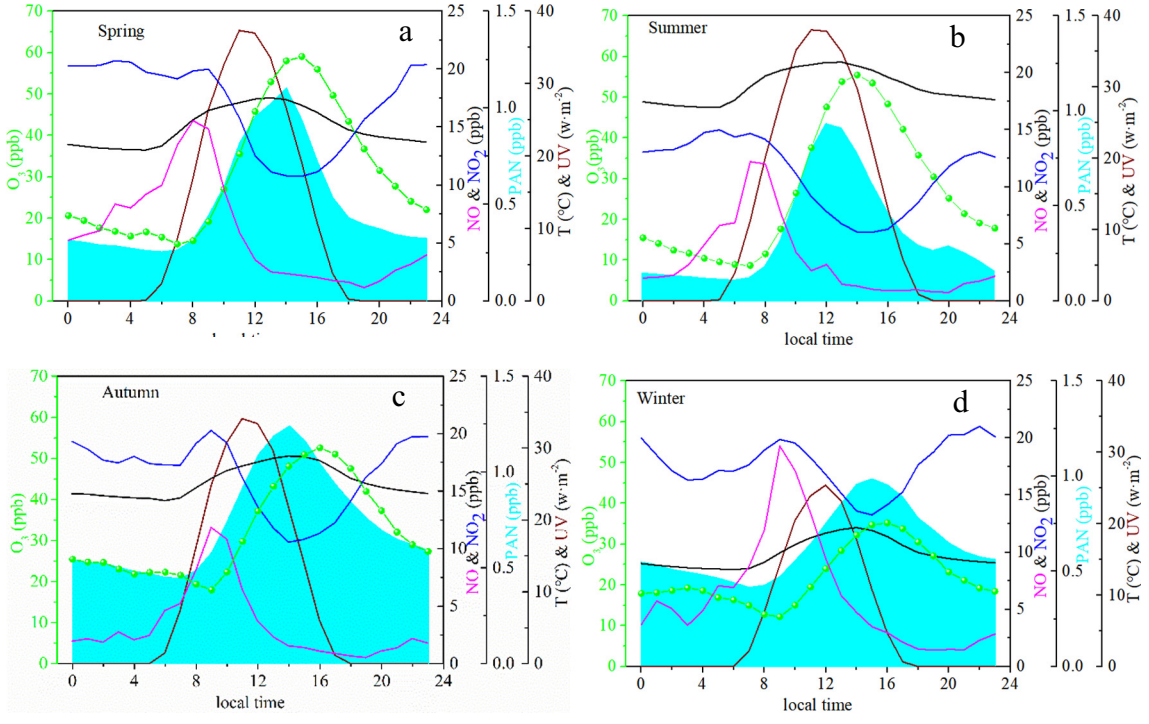

Fig. 2. Average diurnal patterns of PAN, O_3 and related parameters in spring (a), summer (b), autumn (c) and winter (d).

2004). Therefore, we explored what factors affect the fate of PAN in different seasons based on the correlation between PAN and O_3. Fig. 3 showed moderate correlations between hourly concentration of PAN and O_3 in spring ($R^2 = 0.41$) and summer ($R^2 = 0.45$), while weak correlations between PAN and O_3 in autumn ($R^2 = 0.30$) and winter ($R^2 = 0.21$) were found. It was proved by Fig. S1 that thermal degradation is an important pathway of the removal of PAN. As shown in Fig. S1, daily maximum O_3 concentration was positively correlated with daily maximum temperature, while there was no significant correlation between daily maximum PAN and daily maximum temperature. If thermal degradation was taken into account, the daily maximum temperature had a significant positive correlation with the daily maximum PAN +TPAN (thermal decomposition of PAN). The calculation of TPAN has been described in the previous study (Grosjean et al., 2002). In this study, the correlations between hourly concentrations PAN+TPAN and O_3 were better than those of PAN and O_3 (Fig. 3). Compared with

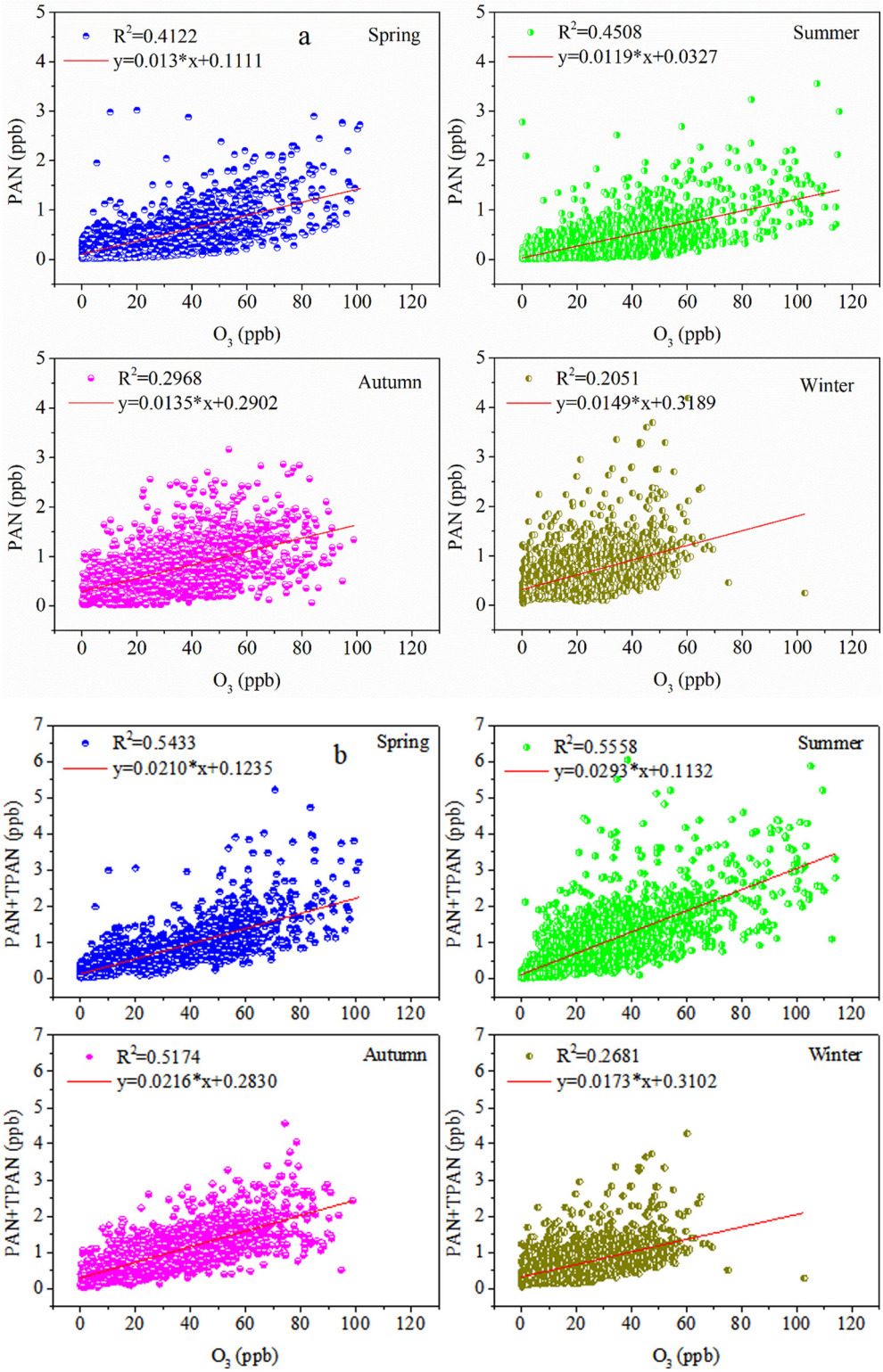

Fig. 3. Scatter plots of PAN versus O_3 (a) and PAN+TPAN versus O_3(b) in Xiamen in different seasons.

other seasons ($R^2 \geq 0.5174$), the correlation between PAN+TPAN and O_3 was weak in winter ($R^2 = 0.2681$). Except for temperature, there were other factors affecting the correlation between PAN and O_3 in winter. When the NO titration was taken into account, the R^2 between O_X ($O_3 + NO_2$) and PAN+TPAN increased from 0.2681 to 0.4683 in winter (Fig. 4). In addition, atmospheric boundary layer exhibits a stable state in winter, which is not conducive to the diffusion of air pollutants. NO was rapidly reacted with O_3 to decrease the concentration of O_3, resulting in a weaker correlation between PAN and O_3 (Zhang, 2013; Zhang et al., 2014).

3.4. PAN/O_3 concentrations correlated with their precursors and environmental factors

To explore key factors affecting photochemical pollution, we analyzed the correlations of PAN and O_3 concentration with other parameters. The monitoring period were divided into two groups, one group for UV > 0 with photochemical reactions, another for UV = 0 without photochemical reactions. Pearson correlation coefficients were shown in Table 3. Higher correlation coefficient of PAN and O_3 was found under the UV > 0 conditions. Meanwhile, the correlation coefficients between O_3 and NO were much higher than those of PAN and NO both UV > 0 and UV = 0. In this study, one of the main removal pathways of O_3 was NO titration, while the removal of PAN was thermal degradation. Thermal degradation of PAN could cause the formation of PA. The process of chemical reaction that NO was reacted with PA would enhance the removal of PAN. If PA continued to combine with NO_2, PAN was generated again. This could be proved by a significantly negative correlation between PAN and temperature, and a significantly positive correlation with NO_2 under the UV = 0 condition.

During the whole monitoring period, the significantly positive correlation between PAN and different particle sizes particles, including PM_1, $PM_{2.5}$, and PM_{10}, were found in both UV > 0 and UV = 0. It was reported by Zhang et al. (2019) that high PAN concentrations accompanied by high particulate matter (PM) concentration was related to the increase of HONO concentration, but the mechanism is not clear. In this study, we simultaneously monitored HONO concentration to further verify the hypothesis. As shown in Fig. S2, the positive correlations between HONO and $PM_{2.5}$ were found in both daylight ($R^2 = 0.13$) and nighttime ($R^2 = 0.18$). Moreover, significant correlation between OH radical and HONO × JHONO was found ($P < 0.05$) based on the monitoring data in December. The results proved that OH radical could be enhanced by HONO photolysis. More heterogeneous transformation of NO_2 to HONO on the surface of PM would result in the increase of HONO (Liu et al., 2014). Much OH radicals originated from HONO accordingly contributed to the faster generation of PAN (Fu et al., 2019). This was consistent with the findings that significantly positive correlation between HONO * JHONO with PAN was found.

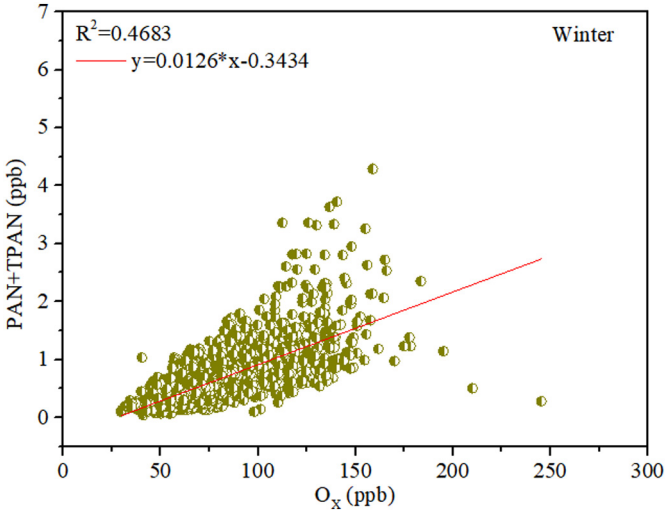

Fig. 4. Scatter plots of PAN+TPAN versus O_X in winter in Xiamen.

Table 3
Correlations of PAN and O_3 concentrations with other parameters.

	PAN		O_3	
	UV > 0	UV = 0	UV > 0	UV = 0
O_3	0.561**	0.421**	1	1
PAN	1	1	0.561**	0.421**
NO	−206**	−0.156**	−0.480**	−0.430**
NO_2	0.000	0.228**	−0.481**	−0.386**
PM_1	0.324**	0.382**	0.219**	0.144**
$PM_{2.5}$	0.250**	0.393**	0.044**	0.022
PM_{10}	0.243**	0.363**	0.042**	−0.016
HONO * JHONO	0.123**	–	0.054**	–
RH	−0.484**	−0.404**	−0.472**	−0.408**
UV	0.303**	–	0.247**	–
JNO_2	0.143**	–	0.304**	–
T	−0.083**	−0.380**	0.339**	0.027
WS	0.091**	0.132**	0.316**	0.210**

Note: "–" indicated that there was no sense for correlation analysis.
** The significance level is 0.01.

Under the UV > 0 or UV = 0 conditions, PAN and O_3 were significantly negatively correlated with relative humidity. High relative humidity was often accompanied by rainfall or cloudy (Lee et al., 2013), which resulted in very weak radiation and might remove the precursors of PAN and O_3 by wet deposition. In addition, PAN and O_3 were significantly positively correlated with UV and JNO_2, which indicated that local photochemical reaction played an important role in the concentration of PAN and O_3 (Sadanaga et al., 2019). Detail analysis of local generation would be conducted in the case study (see Section 3.6). Besides, PAN and O_3 were significantly positively correlated with wind speed, suggesting the impact of regional transport (Li et al., 2016).

3.5. The effect of transport on O_3 and PAN

Bivariate polar plots were applied to demonstrate how the wind speed and wind direction affect the concentrations of PAN and O_3. The bivariate polar plot of PAN and O_3 were shown in Fig. 5, where hourly data points of PAN and O_3 were shown on color-coded. The result indicated that PAN and O_3 concentrations were the highest when the prevailing wind direction is the south wind. Downtown area in Xiamen with big population and large number of vehicles lies to the south of the monitoring site. When the southerly wind blows, the exhaust (including VOCs and NOx) from vehicles might contribute to the formation of PAN and O_3 in suburban area. Except for precursors, the removal pathway and lifetime of PAN and O_3 are not exactly the same. Therefore, distribution pattern of O_3 and PAN was different (Fig. 5). It could be proved by the spatial distribution of O_3 that when the southerly wind was blown (Fig. S3 & Fig. S4), the O_3 concentration of the downwind direction of Xiamen island was significantly higher than that of Xiamen island. It was usually observed that increase in O_3 concentration as the wind speed increased in all the four seasons (Fig. 5b). Under calm weather conditions ($WS < 2\ m \cdot s^{-1}$), the concentration of NO in the atmosphere was high (Fig. S5), and the titration effect on ozone was obvious. However, the precursors were gradually converted into stable product-O_3 during the transport. PAN concentration also increased with the increasing of WS in winter, which was stable under colder environment. In contrast, low PAN concentration with wind speed $>2\ m \cdot s^{-1}$ in summer, reflecting the diffusion of PAN affected by the clean air mass from the ocean.

Backward trajectory analyses were further applied to explore the effect of long-range transport on the concentrations of PAN and O_3 (Ahamad et al., 2014). In this study, we calculated 72 h backward trajectories of air mass reaching the monitoring site. These trajectories were divided into four clusters in different seasons. Fig. 6 and Table 4 showed

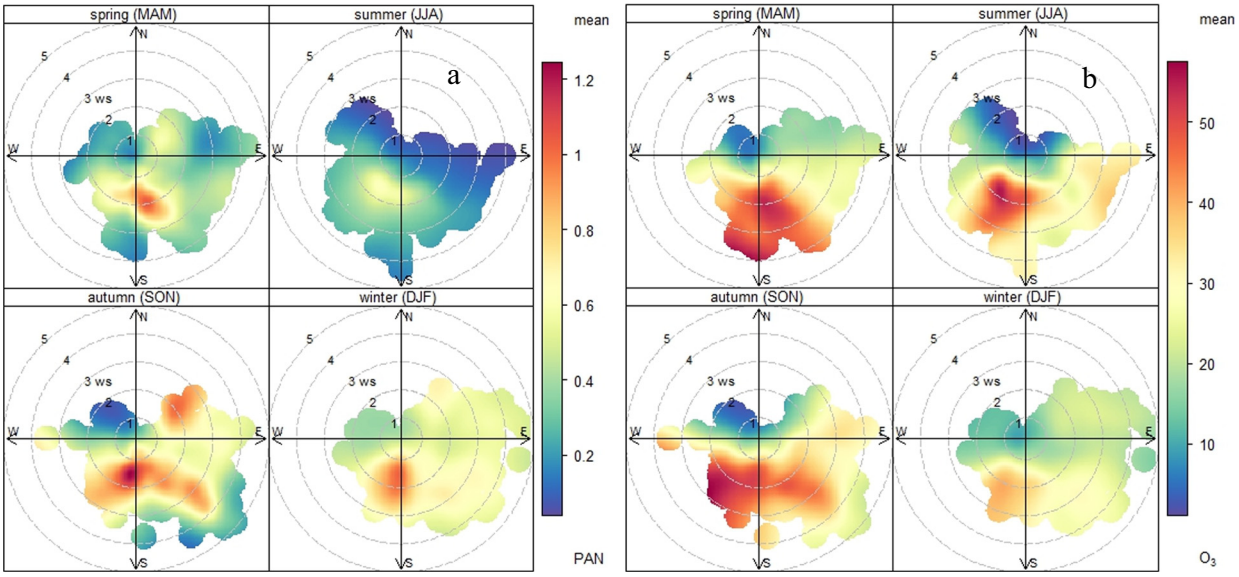

Fig. 5. Bivariate plot of PAN concentrations (a) and O_3 concentrations (b), respectively.

the clusters of trajectories and the concentrations of air pollutants from different clusters, respectively. Backward trajectory clusters in spring were shown in Fig. 6a. Cluster 1 represented the trajectories came from South China Sea. Cluster 2 represented the trajectories originating from the Hebei, and passing through heavily polluted regions in East China Coast, such as Shandong, Jiangsu, Zhejiang, and Fujian province. Cluster 3 originated from East China Sea and cluster 4 came from the Pacific Ocean. Backward trajectory clusters in summer were shown in Fig. 6b. Cluster1 and cluster 2 represented the trajectories came from East China Sea and South China Sea, respectively. Cluster 3 represented

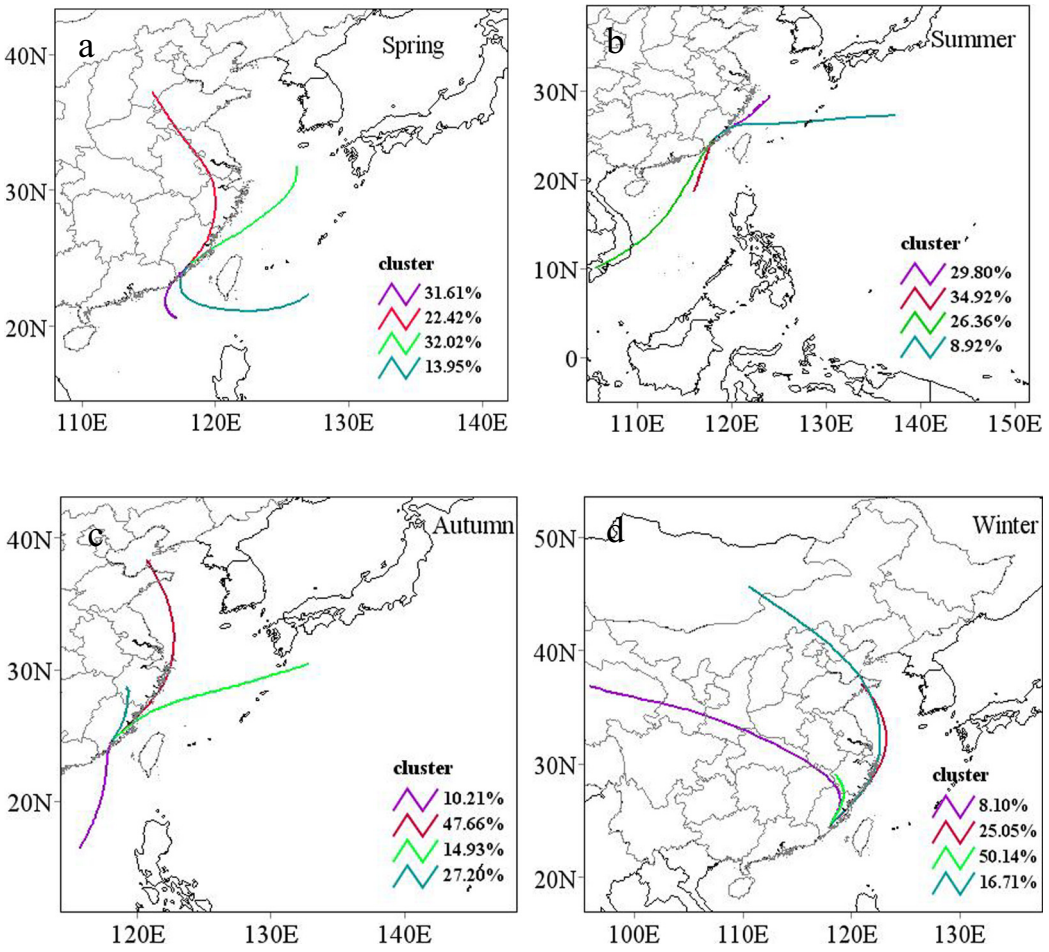

Fig. 6. Mean backward trajectory clusters of spring (a), summer (b), autumn (c), and winter (d).

Table 4
Corresponding mean concentrations of PAN, O_3, CO, and $PM_{2.5}$ of the cluster for each season.

		PAN (ppb)	O_3 (ppb)	CO (ppb)	$PM_{2.5}$ ($\mu g \cdot m^{-3}$)
Spring	Cluster1	0.41	28.76	480.15	35.76
	Cluster2	0.67	36.20	420.96	33.03
	Cluster3	0.60	34.72	418.18	40.12
	Cluster4	0.22	19.77	393.86	34.05
Summer	Cluster1	0.43	34.38	425.77	21.14
	Cluster2	0.38	27.55	470.59	23.82
	Cluster3	0.23	18.17	468.03	15.02
	Cluster4	0.25	21.09	361.13	10.71
Autumn	Cluster1	0.43	26.81	436.99	23.45
	Cluster2	0.80	37.46	404.67	23.35
	Cluster3	0.34	23.67	367.69	18.62
	Cluster4	0.90	30.05	481.37	37.29
Winter	Cluster1	0.76	20.98	401.41	31.36
	Cluster2	0.48	22.51	381.77	33.86
	Cluster3	0.72	22.03	470.13	48.26
	Cluster4	0.56	22.49	350.66	23.55

the trajectories originating from Vietnam and passing through South China Sea. Cluster 4 represented trajectories came from the Pacific Ocean. Backward trajectory clusters in autumn were shown in Fig. 6c. Cluster1 and cluster 3 represented marine air mass originating from South China Sea and the Pacific Ocean, respectively. Cluster 2 originated from Bohai Bay region passing through Shandong, Yellow Sea, and Fujian province. Cluster 4 represented trajectories came from Fujian Province. Backward trajectory clusters in winter were shown in Fig. 6d. Cluster 1 and cluster 3 were the representative of long-range and short-range continental air mass, respectively. Cluster 2 and cluster 4 represented mesoscale and long-range coastal air mass, respectively.

The cluster 4 in spring, the cluster 3 & cluster 4 in summer, and the cluster 3 in autumn were all the clean air mass from the ocean, representing low concentration of PAN (0.22–0.34 ppb) and O_3 (18.17–23.67 ppb). The cluster 4 in autumn and the cluster 3 in winter represent continental trajectories that moved slow, and high concentrations of PAN (0.90 and 0.72 ppb, respectively) were observed. Both of them were characterized by high CO concentration and $PM_{2.5}$ concentration (Table 1). The cluster 1 in spring and the cluster 1 & cluster 2 in summer accompanied by medium PAN concentration (ranging from 0.38 to 0.43 ppb) represented the trajectories from developed coastal area of East China.

3.6. Case study of PAN pollution

3.6.1. Time series of PAN, O_3 and other parameters

During 13–25 Dec., 2018, PAN concentration in Xiamen was often higher than 1.0 ppb, reaching a maximum of 4.2 ppb in 22 Dec., 15:00 (Fig. 7). Even in winter, high concentration of PAN was still a non-negligible part of air pollution in coastal area of southeast China. Criteria air pollutants such as O_3 and particulate matter play a decisive role in the formation of PAN (Xue et al., 2014). In this study, high concentration of PAN was often accompanied by haze pollution (mean wind speed was 1.18 $m \cdot s^{-1} < 2\ m \cdot s^{-1}$ during 17–22 Dec.). Similar phenomenon was found in Seoul by Han et al. (2017). Previous studies reported that PAN and O_3 had similar sources, which might come from regional transport or derive from local photochemical generation (Wang et al., 2015). Air pollutants, such as NO and NO_2, could affect the occurrence and fate of PAN and O_3 (Lin et al., 2011).

3.6.2. Meteorological condition

The meteorological condition plays a vital role in the accumulation or transport of air pollutants (Lu et al., 2019; Wu et al., 2019; Zhao and Wang, 2017). In this study, the monitoring site was under the control of the northerly wind in the front of the cold high pressure on 13, Dec., 2018 (Fig. 8a). There was no sunshine all day with 0.1 mm rainfall and with low temperature (Table 5). The concentrations of PAN, O_3 and other pollutants were low. The cold high pressure moved eastward into the overhead of sea, and turned to the southeast wind control on 14, Dec., 2018 (Fig. 8b). The temperature rose remarkably and sunshine duration increased from 1.2 h on the 14th to 6.3 h on the 15th. The concentrations of PAN, O_3 and other pollutants were still low, due to the favorable atmospheric diffusion conditions. On the 16th, before the arrival of a new cold air, temperature continued to rise with weak precipitation in the warm zone. $PM_{2.5}$ concentration increased due to weak atmospheric diffusion conditions. Strong cold air swept from the south again in 17th. Therefore, the monitoring site was under the control of strong cold and high pressure and the northerly airflow strengthened (Fig. 8c). The minimum temperature dropped significantly, and the sunshine duration significantly increased to 9–10 h. Range of daily

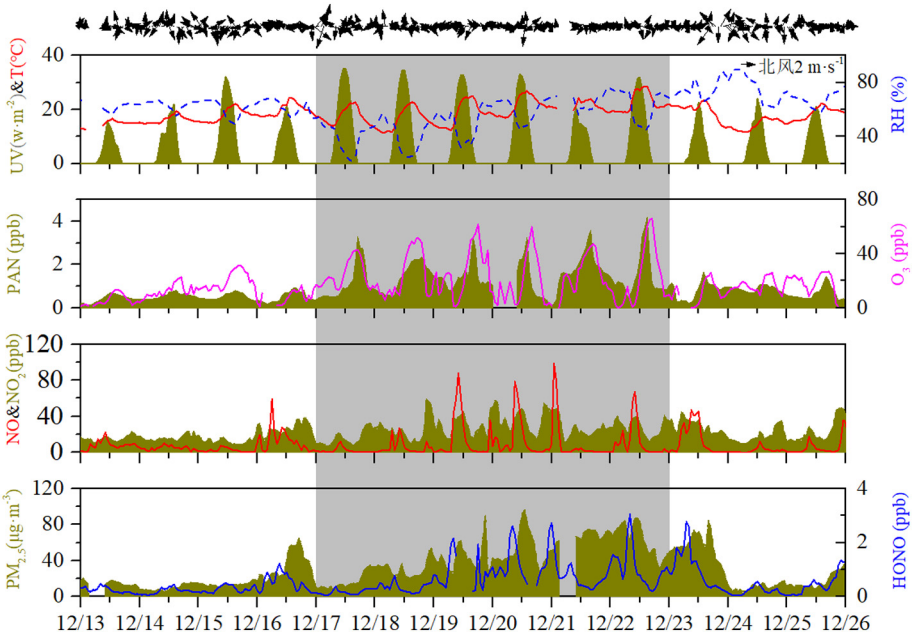

Fig. 7. Time series of PAN, O_3 and other parameters during 13–25 Dec., 2018.

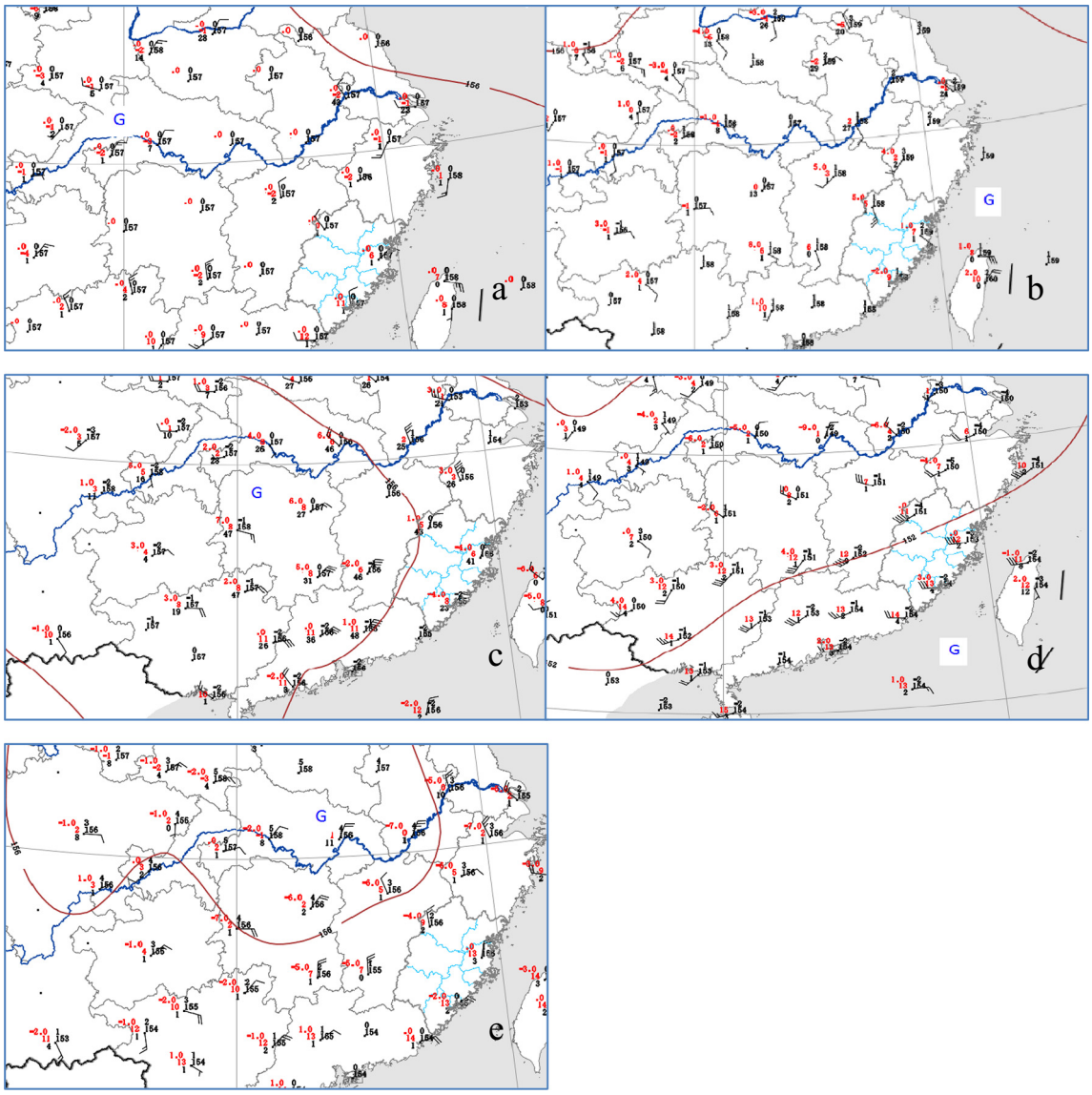

Fig. 8. 08 h 850 hPa height meteorological field on 13 (a), 14 (b), 17 (c), 20 (d), and 23 (e) Dec., 2018.

temperature was 6–8 °C. This was not only conducive to the photochemical reaction to generate PAN during the daytime, but also in favor of the accumulation of PAN during the nighttime. As the high-pressure center gradually entered the surface of the sea, the monitoring site was controlled by the southwest airflow in the back of the high pressure in the 19th and 20th (Fig. 8d). The UV radiation was further strengthened, the temperature continued to rise, the relative humidity decreased, and sunshine duration was long, and daily temperature range was large (11.2 °C). These conditions were favorable for photochemical reactions, so the daily maximum concentrations of PAN and O_3 were above 3 ppb and 60 ppb, respectively. Besides, daily maximum concentration of $PM_{2.5}$ also increased to 80 $\mu g \cdot m^{-3}$. The weather was

Table 5
Statistics on meteorological parameters in Xiamen city (59134 Station) on 13–25, Dec., 2018.

Date (MM/DD)	08-08 precipitation (mm)	Sunshine duration (hour)	Maximum temperature (°C)	Minimum temperature (°C)	Daily temperature range
12/13	0.1	0	15.2	11.3	5.3
12/14		1.2	17.5	13.8	3.9
12/15		6.3	20.3	14.3	6.0
12/16	0.0	0	20.9	15.7	6.0
12/17		9.3	19.7	13.5	6.2
12/18		10.0	19.8	11.7	8.1
12/19		9.6	22.3	11.1	11.2
12/20	0.0	8.3	24.1	15.0	11.2
12/21		0.9	21.1	16.7	9.1
12/22		9.6	26.4	16.8	9.6
12/23	21.6	0	21.4	14.8	9.6
12/24	1.3	0	15.6	11.5	6.6
12/25	0.3	0	18.2	14.8	4.1

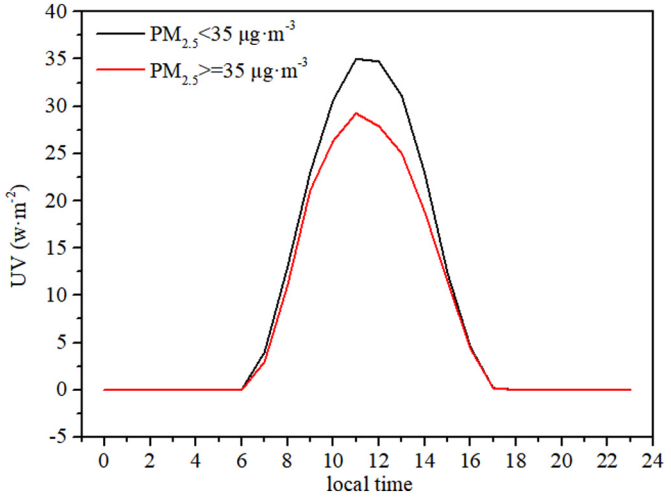

Fig. 9. Diurnal variation in the ultraviolet radiation (UV) from 17, Dec., 2018 to 22, Dec. 2018 grouped by $PM_{2.5}$ concentrations.

calm in Xiamen and the $PM_{2.5}$ concentration continued to increase under the control of the transformed surface cold high and warm sector ahead of front. Xiamen experienced a high temperature (26.4 °C) and a sunshine duration was 9.6 h on the 22nd under the control of the warm front before the new cold air swept from the south. The daily maximum value of PAN and O_3 was 4.19 ppb and 66.08 ppb, respectively. A new cold air swept from Xiamen (Fig. 8e) and resulted in heavy rainfall (21.6 mm) on the 23rd (Table 5). It continued to rain in the next two days, the temperature was low, and the sunshine duration was 0. Therefore, the concentrations of PAN and O_3 were low during 23–25th Dec., 2018.

3.6.3. The effect of $PM_{2.5}$ on PAN

Fig. 9 showed diurnal variation of UV from 17, Dec., 2018 to 22, Dec. 2018 with respect to the $PM_{2.5}$ concentration. At noon, the value of UV with low $PM_{2.5}$ concentration (<35 $\mu g \cdot m^{-3}$) was significantly higher than that with high $PM_{2.5}$ concentration (≥35 $\mu g \cdot m^{-3}$). The maximum difference is 6.86 $w \cdot m^{-2}$ at 12:00, indicating the influence of $PM_{2.5}$ through scattering and absorption (Wang et al., 2019). Zhang et al. (2019) reported that the reactivity of OH radicals was dominated in the oxidation VOCs and NOx rather than by UV in urban area. In clean atmosphere, the leading OH radical daytime source was commonly from O_3 photolysis with H_2O, while in polluted air, the HONO photolysis was the potential source of OH radicals (Lu et al., 2013). Reaction (1) was the specific formula of HONO photolysis to form OH radicals.

$$HONO + h\nu \rightarrow OH + NO(300nm<\lambda<400nm) \quad (1)$$

Table 6
The PAN lifetimes and related reaction rate constants at different situations.

Condition	k_2 ($\times 10^{-11}$)	k_{-2} ($\times 10^{-4}$)	k_3 ($\times 10^{-11}$)	T(°C)	NO/NO_2	L (day)
Spring&$PM_{2.5}$ < 35	1.198	7.626	2.005	24.258	0.138	0.730
Spring&$PM_{2.5}$ ≥ 35	1.195	7.440	2.010	23.509	0.204	0.848
Summer&$PM_{2.5}$ < 35	1.218	14.5	1.972	29.694	0.199	0.144
Summer&$PM_{2.5}$ ≥ 35	1.231	24.4	1.952	33.296	0.147	0.074
Autumn&$PM_{2.5}$ < 35	1.202	8.656	1.997	25.495	0.098	1.165
Autumn& $PM_{2.5}$ ≥ 35	1.200	8.055	2.001	24.908	0.110	1.170
Winter&$PM_{2.5}$ < 35	1.165	1.805	2.062	15.224	0.175	1.630
Winter&$PM_{2.5}$ ≥ 35	1.169	2.273	2.055	16.413	0.225	3.246

Note: T is the abbreviation of temperature, and L is the abbreviation of lifetime.

In this study, the HONO concentration was correlated positively with $PM_{2.5}$ with $R^2 = 0.13$ (Fig. 10a). The result was consistent with Bao et al. (2018) and Liu et al. (2014). We also found that the mean value (0.94 ppb) of HONO concentration with $PM_{2.5}$ ≥ 35 $\mu g \cdot m^{-3}$ was much higher than that (0.38 ppb) with $PM_{2.5}$ < 35 $\mu g \cdot m^{-3}$. High levels of HONO resulted in more OH radicals to enhance the faster formation of PAN. The high concentration of O_3 further verified strong photochemical reactions in this stage. As shown in Fig. 10 b, there was a significant linear correlation ($R^2 = 0.28$) between PAN and O_3.

3.6.4. The lifetime of PAN

The lifetime of PAN was calculated to further discuss the formation reactions and decomposition reactions PAN. The specific calculation of PAN lifetime was introduced in the previous study (Liu et al., 2018). In this study, with high and low $PM_{2.5}$ concentration (≥35 $\mu g \cdot m^{-3}$ and < 35 $\mu g \cdot m^{-3}$, respectively), the lifetime of PAN in winter were 3.246 and 1.630 days, which were approximately 43.86 and 11.32 times longer than those in summer, respectively (Table 6).

4. Conclusions

PAN was continuously monitored in a southeast coastal city to investigate photochemical mechanism and pollution process. PAN concentration in Xiamen was higher than those in remote and regional background sites. Mean concentration of PAN in autumn was significantly higher than all other seasons, and winter was close to autumn, indicating that photochemical pollution was still non-negligible in the cold season. There was 1–2 h time in advance the peak occurrence between PAN and O_3, due to the impact of temperature on the decomposition

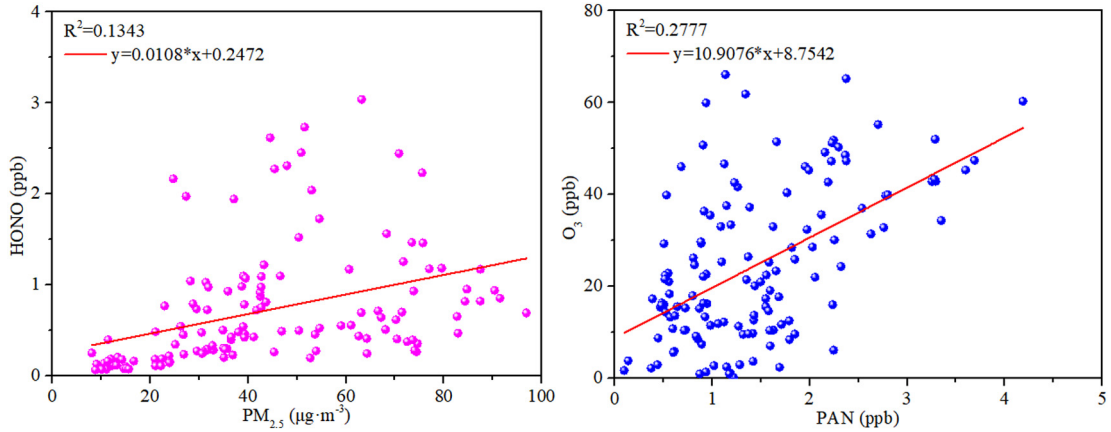

Fig. 10. Linear regression of HONO with $PM_{2.5}$ (a) and PAN with O_3 (b).

rate of PAN. Long-range marine air mass with low concentration of PAN and O_3 was attributed to the diffusion of wind, while continental trajectories with high PAN concentration were characterized by high CO concentration and $PM_{2.5}$ concentration. High concentrations of PAN were attributed to strong photochemical reactions and local accumulation. The long lifetime of PAN in winter under the condition of high $PM_{2.5}$ concentration ($\geq 35\ \mu g \cdot m^{-3}$) favored the accumulation of PAN. Heterogeneous reactions on the $PM_{2.5}$ surface played an important role in the formation of PAN. High concentrations of HONO, sufficient UV and high concentrations of precursors (VOCs and NO_2) were conducive to the promotion of PAN photochemical production in coastal area of southeast China.

CRediT authorship contribution statement

Baoye Hu: Conceptualization, Methodology, Software, Formal analysis, Data curation, Writing - original draft, Visualization.**Taotao Liu:**Formal analysis.**Youwei Hong:**Conceptualization, Methodology, Writing - review & editing.**Lingling Xu:**Software.**Mengren Li:**Conceptualization.**Xin Wu:** Visualization.**Hong Wang:**Resources.**Junhuai Chen:**Methodology. **Jinsheng Chen:**Conceptualization, Methodology, Writing - review & editing, Supervision, Project administration, Funding acquisition.

Declaration of competing interest

The authors declare that there is no conflict of financial interest.

Acknowledgments

This study was funded by the Chinese Academy of Sciences Interdisciplinary Innovation Team Project, the National Key Research and Development Program (2016YFC02005 & 2016YFC0112200), and the National Natural Science Foundation of China (41575146).

Appendix A. Supplementary data

Supplementary data to this article can be found online at https://doi.org/10.1016/j.scitotenv.2020.137493.

References

Ahamad, F., Latif, M.T., Tang, R., Juneng, L., Dominick, D., Juahir, H., 2014. Variation of surface ozone exceedance around Klang Valley, Malaysia. Atmos. Res. 139, 116–127. https://doi.org/10.1016/j.atmosres.2014.01.003.

Bao, F., Li, M., Zhang, Y., Chen, C., Zhao, J., 2018. Photochemical aging of Beijing urban $PM_{2.5}$: HONO production. Environ Sci Technol 52, 6309–6316. https://doi.org/10.1021/acs.est.8b00538.

Duan, J., et al., 2018. Development of an incoherent broadband cavity-enhanced absorption spectrometer for in situ measurements of HONO and NO_2. Atmos Meas Tech 11, 4531–4543. https://doi.org/10.5194/amt-11-4531-2018.

Fu, X., et al., 2019. The significant contribution of HONO to secondary pollutants during a severe winter pollution event in southern China. Atmos. Chem. Phys. 19, 1–14. https://doi.org/10.5194/acp-19-1-2019.

Grosjean, E., Grosjean, D., Woodhouse, L.F., Yang, Y.-J., 2002. Peroxyacetyl nitrate and peroxypropionyl nitrate in Porto Alegre, Brazil. Atmos. Environ. 36, 2405–2419.

Han, J., Lee, M., Shang, X., Lee, G., Emmons, L.K., 2017. Decoupling peroxyacetyl nitrate from ozone in Chinese outflows observed at Gosan Climate Observatory. Atmos. Chem. Phys. 17, 10619–10631. https://doi.org/10.5194/acp-17-10619-2017.

Hu, B., et al., 2019. Characteristics and formation mechanism of surface ozone in a coastal island of Southeast China: influence of sea-land breezes and regional transport. Aerosol Air Qual. Res. 19, 1734–1748. https://doi.org/10.4209/aaqr.2019.04.0193.

Lee, G., Jang, Y., Lee, H., Han, J.S., Kim, K.R., Lee, M., 2008. Characteristic behavior of peroxyacetyl nitrate (PAN) in Seoul megacity, Korea. Chemosphere 73, 619–628. https://doi.org/10.1016/j.chemosphere.2008.05.060.

Lee, G., Choi, H.-S., Lee, T., Choi, J., Park, J.S., Ahn, J.Y., 2012. Variations of regional background peroxyacetyl nitrate in marine boundary layer over Baengyeong Island, South Korea. Atmos. Environ. 61, 533–541. https://doi.org/10.1016/j.atmosenv.2012.07.075.

Lee, J.-B., et al., 2013. Peroxyacetyl nitrate (PAN) in the urban atmosphere. Chemosphere 93, 1796–1803. https://doi.org/10.1016/j.chemosphere.2013.06.019.

Li, Y., et al., 2016. Observation of regional air pollutant transport between the megacity Beijing and the North China Plain. Atmos. Chem. Phys. 16, 14265–14283. https://doi.org/10.5194/acp-16-14265-2016.

Lin, W., Xu, X., Ge, B., Liu, X., 2011. Gaseous pollutants in Beijing urban area during the heating period 2007–2008: variability, sources, meteorological, and chemical impacts. Atmos. Chem. Phys. 11, 8157–8170. https://doi.org/10.5194/acp-11-8157-2011.

Liu, L., et al., 2018. Understanding unusually high levels of peroxyacetyl nitrate (PAN) in winter in Urban Jinan, China. J. Environ. Sci. (China) 71, 249–260. https://doi.org/10.1016/j.jes.2018.05.015.

Liu, Z., et al., 2014. Evidence of aerosols as a media for rapid daytime HONO production over China. Environ Sci Technol 48, 14386–14391. https://doi.org/10.1021/es504163z.

Lu, K.D., et al., 2013. Missing OH source in a suburban environment near Beijing: observed and modelled OH and HO_2 concentrations in summer 2006. Atmos. Chem. Phys. 13, 1057–1080. https://doi.org/10.5194/acp-13-1057-2013.

Lu, S., Hu, Q., Wu, S., Wang, X., Chen, X., 2014. Establishment of air pollutant emission inventory in the West Coast of Taiwan Strait. Acta Sci. Circumst. 34, 2624–2634.

Lu, X., et al., 2019. Exploring 2016–2017 surface ozone pollution over China: source contributions and meteorological influences. Atmos. Chem. Phys. 19, 8339–8361. https://doi.org/10.5194/acp-19-8339-2019.

Mellouki, A., Wallington, T.J., Chen, J., 2015. Atmospheric chemistry of oxygenated volatile organic compounds: impacts on air quality and climate. Chem. Rev. 115, 3984–4014. https://doi.org/10.1021/cr500549n.

Qiu, Y., Ma, Z., Li, K., 2019. A modeling study of the peroxyacetyl nitrate (PAN) during a wintertime haze event in Beijing, China. Sci. Total Environ. 650, 1944–1953. https://doi.org/10.1016/j.scitotenv.2018.09.253.

Rubio, M.A., Oyola, P., Gramsch, E., Lissi, E., Pizarro, J., Villena, G., 2004. Ozone and peroxyacetyl nitrate in downtown Santiago, Chile. Atmos. Environ. 38, 4931–4939. https://doi.org/10.1016/j.atmosenv.2004.05.051.

Sadanaga, Y., et al., 2019. Behavior of total peroxy and total organic nitrate concentrations at Suzu on the Noto peninsula, Japan: long-range transport and local photochemical production. Atmos. Environ. 196, 20–26. https://doi.org/10.1016/j.atmosenv.2018.10.003.

Sillman, S., Samson, P.J., 1995. Impact of temperature on oxidant photochemistry in urban, polluted rural and remote environments. Journal of Geophysical Research: Atmospheres (D6), 100 https://doi.org/10.1029/94JD02146.

Singh, H.B., Salas, L.J., Viezee, W., 1986. Global distribution of peroxyacetyl nitrate. Nature 321, 588–591.

Tanimoto, H., 2002. Seasonal cycles of ozone and oxidized nitrogen species in northeast Asia 1. Impact of regional climatology and photochemistry observed during RISOTTO 1999–2000. J. Geophys. Res. 107. https://doi.org/10.1029/2001jd001496.

Temple, P., Taylor, O., 1983. World-wide ambient measurements of peroxyacetyl nitrate (PAN) and implications for plant injury. Atmos. Environ. 17, 1583–1587.

Wang, B.G., Zhu, D., Zou, Y., et al., 2015. Source analysis of peroxyacetyl nitrate (PAN) in Guangzhou, China: a yearlong observation study. Atmos Chem Phys Discussions 15 (12), 17093–17133.

Wang, W., Li, X., Shao, M., Hu, M., Zeng, L., Wu, Y., Tan, T., 2019. The impact of aerosols on photolysis frequencies and ozone production in Beijing during the 4-year period 2012–2015. Atmos. Chem. Phys. 19, 9413–9429. https://doi.org/10.5194/acp-19-9413-2019.

WHO, 1987. WHO Air Quality Guideline for Europe. Air Quality Guidelines for Europe. WHO Regional Office in Europe, Copenhagen.

WHO, 1996. Update and Revision of the WHO Air Quality Guideline for Europe. Classical Air Pollutant; Ozone and Other Photochemical Oxidants. European Center for Environmental and Health, Bilthoven, Netherlands.

Wu, X., et al., 2019. The air pollution governed by subtropical high in a coastal city in Southeast China: formation processes and influencing mechanisms. Sci. Total Environ. 692, 1135–1145. https://doi.org/10.1016/j.scitotenv.2019.07.341.

Xie, M., et al., 2016. Temporal characterization and regional contribution to O_3 and NOx at an urban and a suburban site in Nanjing, China. Sci. Total Environ. 551–552, 533–545. https://doi.org/10.1016/j.scitotenv.2016.02.047.

Xu, X., Zhang, H., Lin, W., Wang, Y., Xu, W., Jia, S., 2018. First simultaneous measurements of peroxyacetyl nitrate (PAN) and ozone at Nam Co in the central Tibetan Plateau: impacts from the PBL evolution and transport processes. Atmos. Chem. Phys. 18, 5199–5217. https://doi.org/10.5194/acp-18-5199-2018.

Xue, L., et al., 2014. On the use of an explicit chemical mechanism to dissect peroxy acetyl nitrate formation. Environ. Pollut. 195, 39–47. https://doi.org/10.1016/j.envpol.2014.08.005.

Yao, Q., Ma, Z., W-l, L., J-l, L., X-j, W., Z-y, C., S-q, H., 2019. Transport characteristics of PAN and O_3 in the lower atmosphere of the boundary layer in Tianjin in summer. Environmental Science 40, 67–75.

Zeng, L., Fan, G.J., Lyu, X., Guo, H., Wang, J.L., Yao, D., 2019. Atmospheric fate of peroxyacetyl nitrate in suburban Hong Kong and its impact on local ozone pollution. Environ. Pollut. https://doi.org/10.1016/j.envpol.2019.06.004.

Zhang, B., Zhao, X., Zhang, J., 2019. Characteristics of peroxyacetyl nitrate pollution during a 2015 winter haze episode in Beijing. Environ. Pollut. 244, 379–387. https://doi.org/10.1016/j.envpol.2018.10.078.

Zhang, G., et al., 2014. Seasonal and diurnal variations of atmospheric peroxyacetyl nitrate, peroxypropionyl nitrate, and carbon tetrachloride in Beijing. J. Environ. Sci. 26 (1), 65–74. https://doi.org/10.1016/S1001-0742(13)60382-4.

Zhang, G., et al., 2015. Summertime distributions of peroxyacetyl nitrate (PAN) and peroxypropionyl nitrate (PPN) in Beijing: understanding the sources and major sink of PAN. Atmos. Environ. 103, 289–296. https://doi.org/10.1016/j.atmosenv.2014.12.035.

Zhang, H., 2013. Measurement and analysis of peroxyacetyl nitrate (PAN) in the North China region and the Tibetan Plateau [D]. Chinese Academy of Meteorological Science.

Zhang, J.M., et al., 2009. Continuous measurement of peroxyacetyl nitrate (PAN) in suburban and remote areas of western China. Atmos. Environ. 43, 228–237. https://doi.org/10.1016/j.atmosenv.2008.09.070.

Zhao, Z., Wang, Y., 2017. Influence of the West Pacific subtropical high on surface ozone daily variability in summertime over eastern China. Atmos. Environ. 170, 197–204. https://doi.org/10.1016/j.atmosenv.2017.09.024.